Long term monitoring of urban subsidence by Permanent Scatterer DInSAR*

TANG Yixian[1,2], ZHANG Hong[1,2**] and WANG Chao[1,2]

(1. The Chinese Remote Sensing Satellite Ground Station, Chinese Academy of Sciences, Beijing 100086, China; 2. State Key Laboratory of Remote Sensing IRSA, Chinese Academy of Sciences, Beijing 100101, China)

Abstract   When using differential SAR interferometry (DInSAR) to monitor the surface deformation over a long time scale, it is often strongly affected by the spatial and temporal decorrelations and atmospheric dishomogeneities. The recently developed Permanent Scatterers (PS) technique proposed by Fertti et al. can overcome these difficulties by interpreting time-series of interferometric phase only at coherent point scatterers. In this study, we apply this PS technique using 25 ERS-1/2 scenes from 1992 to 2000 to monitor the subsidence in Suzhou. By using the linear deformation model, the deformation map in Suzhou urban area over the eight years is obtained. And the calculated results are in good agreement with the measurements of leveling.

Keywords: Permanent Scatterer, differential SAR interferometry, urban subsidence.

As a new space technique, differential SAR interferometry (DInSAR) can monitor the surface deformation with a high space resolution on day and night[1,2]. However, recent researches show that DInSAR is often limited by the spatial and temporal decorrelations and the atmospheric dishomogeneities[3]. In order to overcome these difficulties, a new technique called Permanent Scatterers (PS) was proposed by Ferretti et al.[4,5], which has been proved to be a powerful and effective tool to explore the Earth surface movement in the urban area. This technique analyzes the phase history of the selected coherent pixels extracted from a stack of N differential interfeograms on the temporal scales. In this paper, PS technique is ultilized to study the subsidence in Suzhou urban area using 25 scenes of ERS-1/2 images from 1992 to 2000. And the deformation map is shown and the result is compared with the leveling measurements.

1 The phase component in DInSAR

Since Refs. [6,7] have given details of the theory and the geometry of InSAR, only the different signal components in DInSAR are emphasized here. Discarding the phase noise caused by registration, the phase at pixel $x = \begin{bmatrix} \xi \\ \eta \end{bmatrix}$ in one SAR image is presented by

$$\psi(x) = \frac{4\pi}{\lambda} r(x) + \sigma(x) + \alpha(x) + n(x), \quad (1)$$

where r is the distance from the satellite to the object, σ is the phase decided by the object scattering, α is the conctribution of atmospheric phase screen (APS), and n is the thermal noise. The phase at x in interferogram is given by

$$\phi(x) = \psi_s(x) - \psi_m(x)$$
$$= \frac{4\pi}{\lambda}[r_s(x) - r_m(x)] + [\sigma_s(x) - \sigma_m(x)]$$
$$+ [\alpha_s(x) - \alpha_m(x)] + n(x), \quad (2)$$

where the suffix m and s represent the master and slave images, respectively, and the repeat orbit r_s is given by

$$r_s = r_m + \Delta r, \quad (3)$$

where Δr is related to the topographic height and the displacement of the object along the direction of radar line of sight (LOS) occurring between two SAR acquisitions:

$$\frac{4\pi}{\lambda}\Delta r = \phi_n + \phi_t$$
$$= \frac{4\pi}{\lambda}\Delta d + \frac{4\pi}{\lambda} \cdot \frac{B_\perp}{R \cdot \sin\theta} \cdot h, \quad (4)$$

where Δd is the displacement of the object, h is the topographic height, $B_\perp$, R and θ are normal baseline, slant range, and the incident angle, respective-

ly. Therefore, the phase in an interferomgram is dependent on the geometry of InSAR, the movement of the object, the scatterer mechanism and the atmosphere change:

$$\phi(x) = \phi_t(x) + \phi_\mu(x) + \phi_a(x)$$
$$+ \phi_\sigma(x) + \phi_n(x), \qquad (5)$$

where $\phi_t(x)$ is the topographic phase, ϕ_μ is the phase related to the deformation along LOS, ϕ_σ is the phase caused by the change of the scatterer, ϕ_a is the phase caused by the atmospheric dishomogeneity, ϕ_n is the thermal noise of the system. $\phi_t(x)$ and ϕ_μ are the geometric phases, and ϕ_σ is the object phase.

Considering DInSAR, we often use an already existing Digtal Elevation Model (DEM) or a DEM estimated from InSAR to remove the topographic phase component. However, because of the imperfectness of the DEM we used, the phase in DInSAR at pixel x is

$$\phi(x) = \phi_{\Delta t}(x) + \phi_\mu(x) + \phi_a(x)$$
$$+ \phi_\sigma(x) + \phi_n(x), \qquad (6)$$

where $\phi_{\Delta t}$ is the residual topographic phase.

Because of the spatial and temporal decorrelations and the atmospheric dishomogeneity, the scatterer phase ϕ_σ and the atmosphere phase ϕ_a cannot be removed perfectly, which even destroys the geometric phase badly. According to Ref. [8], the atmospheric water vapor can introduce 0.68 radian into RMS of interoferometic phase. All of these decorrelation factors prevent the wild applications of the DInSAR technique.

2 PS-DInSAR technique

In 2000, Ferretti et al. proposed a new technique called Permanent Scatterers (PSs) within a multi-image framework to overcome the difficulties in the traditional DInSAR technique, which only exploits the coherent pixels. The coherent pixels are selected from the long time scales and our analysis is only focused on those pixels which can keep coherence over years and contain useful phase information. Here, we just summarize the main steps and focus on the permanent scatterers selection, phase modeling and computing method. Given that the $N + 1$ ERS SAR images of the same area of interest are available, data are first coregistered on a common master image which is selected to minimize the dispersion of the normal baseline values of all the interferogram. Then, the N differential interferograms between all SAR images and the master are computed using an already existing DEM or a DEM estimated from low temporal baseline pairs. When N differential interferograms are available, the residual phase of coherent pixel x in interferogram i without the scatterer phase, which is subtracted during interferometry, is given by

$$\phi(x) = \phi_{\Delta t}(x) + \phi_u(x) + \phi_a(x) + \phi_n(x). \qquad (7)$$

The Permanent Scatterers are identified from the stack of SAR calibration images using amplitude dispersion index considering the scatterers with low value both on amplitude dispersion index and coherence. When the algorithm of amplitude dispersion index (ADI) proposed by Ferretti et al. is applied to the selection of permanent scatterers, the pixels in the shallow area or in the water area are often selected as PSs because of the low variation of the amplitude in calibration of images. To remove these pixels from PSs, two criteria are applied: on the one hand, the amplitude dispersion index is below a threshold, on the other hand, the amplitude is above another threshold in at least N_1 images of all the available SAR images.

$$D_{A\_i} = \frac{\sigma_{A\_i}}{m_{A\_i}} < D_{A\_threshold}, \qquad (8)$$

$$\sum_{k=1}^{N+1} N_{k\_i} > N_{threshold}$$
$$\begin{cases} N_{k\_i} = 1, & \text{when } A_{k\_i} \geqslant A \\ N_{k\_i} = 0, & \text{when } A_{k\_i} \geqslant A \end{cases}; \qquad (9)$$

where m_{A_i} and σ_{A_i} are the mean and the standard deviations of the amplitude value for each pixel on the time scale, $D_{A\_threshold}$ is the threshold of DAI, A is the threshold of amplitude, and $m_{A\_k} + \sigma_{A\_k}$ is the threshold amplitude above which every pixel should be.

For the purpose of deformation extraction, the phase variation between neighboring PSs is considered to cancel the different phase offsets among differential interferograms. At the same time, the atmospheric phase is much reduced because of the correlation between the tow closed PSs[9]. Considering the linear deformation, it is possible to retrieve a good estimation of them by adjusting the following phase model to data

$$\phi_{ij}^k = 4\pi \cdot \frac{\Delta v_{ij} \cdot T^k}{\lambda} + \frac{4\pi}{\lambda} \cdot \frac{B_\perp^k \cdot \Delta\epsilon_{ij}}{R_i^k} \cdot \frac{1}{\sin\theta} + \omega^k, \qquad (10)$$

where ϕ_{ij}^{k} is the phase difference between PS pixel i and j, Δv_{ij} and $\Delta\varepsilon_{ij}$ are the increments of deformation velocity and the height error between PS i and j, T^{k} and $B_{\perp}^{k}$ are the temporal and normal baselines, respectively, and ω^{k} is the linear residual phase. The model adjustment function, namely the coherence function, is maximized to find the value of Δv_{ij} and $\Delta\varepsilon_{ij}$:

$$
\begin{aligned}
\gamma_{ij} &= \frac{1}{N}\sum_{k=1}^{N} | \exp[j(\phi_{ij}^{k} - \hat{\phi}_{ij}^{k})] | \\
&= \frac{1}{N}\sum_{k=1}^{N} \left| \exp\left[j \cdot \left(\phi_{ij}^{k} - \frac{4\pi}{\lambda}\Delta v_{ij}T^{k} \right.\right.\right. \\
&\quad \left.\left.\left. - \frac{4\pi}{\lambda}\frac{B_{\perp}^{k}}{R}\frac{\Delta\varepsilon_{ij}}{R}\cdot\frac{1}{\sin\theta}\right)\right]\right|.
\end{aligned}
\tag{11}
$$

The maximization of γ_{ij} is equivalent to finding the bidimensional frequency of the complex sinusoid derived from the phase term[10]. This can be accomplished using one of the well known techniques developed in spectral analysis. Once the values for all PSs are found, the final solution of each PS is obtained through an integration process and the deformation map is also obtained by Kriging interpolation.

3 Experiment and discussion

To validate the proposed PS algorithm, the urban area of Suzhou is selected as the test area because of its subsidence due to excessive groundwater pumping[11]. 25 ERS SAR images gathered over the area from 1992 to 2000 are co-registered on the common master (ERS-1 orbit 23309 taken on December 30, 1995). The basic information about the images is given in Table 1. The temporal baseline is over 8 years and the baseline exceeds 2000 meters. Fig. 1 is the average amplitude image of the urban area that our test is focused on, which is about 18 km × 18 km. Fig. 2 is the interferogram acquired by the master and the image of ERS-2 orbit 24311 taken on December 31, 1995.

Table 1.   ERS-1/2 data set of Suzhou area

No.	Orbit	Date	T^{k}(days)	$B_{\perp}^{k}$(m)	No.	Orbit	Date	T^{k}(days)	$B_{\perp}^{k}$(m)
1	E1-23309	1995-12-30	0	0	14	E2-14658	1998-02-08	771	− 792
2	E1-7434	1992-12-17	− 1108	− 2240	15	E2-15159	1998-03-15	806	− 614
3	E1-8436	1993-02-25	− 1038	36	16	E2-15660	1998-04-19	841	− 331
4	E1-8937	1993-04-01	− 1003	− 11	17	E2-16662	1998-06-28	911	− 1329
5	E1-9939	1993-06-01	− 933	− 901	18	E2-18165	1998-10-11	1016	− 132
6	E1-10440	1993-07-15	− 898	− 1101	19	E2-19167	1998-12-20	1086	− 828
7	E1-11943	1993-10-28	− 793	175	20	E2-21672	1999-06-13	1261	− 1058
8	E1-12444	1993-12-02	− 758	235	21	E2-23175	1999-09-26	1366	72
9	E1-19802	1995-04-29	− 245	− 957	22	E2-25179	2000-02-13	1506	− 101
10	E1-3636	1995-12-31	1	− 282	23	E2-26682	2000-05-28	1611	305
11	E1-24311	1996-03-09	70	− 21	24	E2-28185	2000-09-10	1716	− 1595
12	E2-4638	1996-03-10	71	78	25	E2-29688	2000-12-24	1821	− 907
13	E2-12153	1997-08-17	596	381					

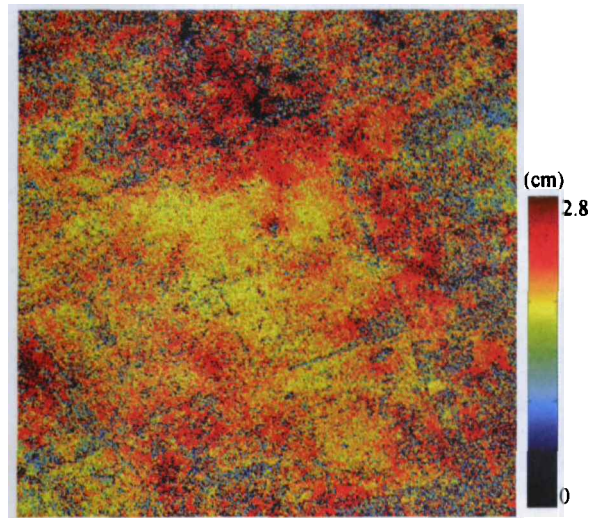Fig. 1.   The amplitude image of the test area in Suzhou.

Fig. 2.   The interferogram acquired by tandem pair.

Using the PS selection algorithm presented in Section 2, 1436 PSs are identified from the stack calibration images. The distribution of these PSs over the amplitude images is presented in Fig.3. By maximizing the adjustment function model, the mean of the subsidence velocity of 2.48 cm/a on LOS is obtained. And the deformation map is shown in Fig.4 using the Kriging interpolation method, which agrees with the result obtained by the traditional DInSAR[12]. The comparison of the result with the leveling measurements observed from 1993 to 1995 at 6 locations labeled in Fig.4 is presented in Table 2. From the result shown in Table 2, we find that the subsidence rate is reduced at those locations (P_1, P_2, P_3, P_4, P_5, P_6) inside the moat where the control project is carried out.
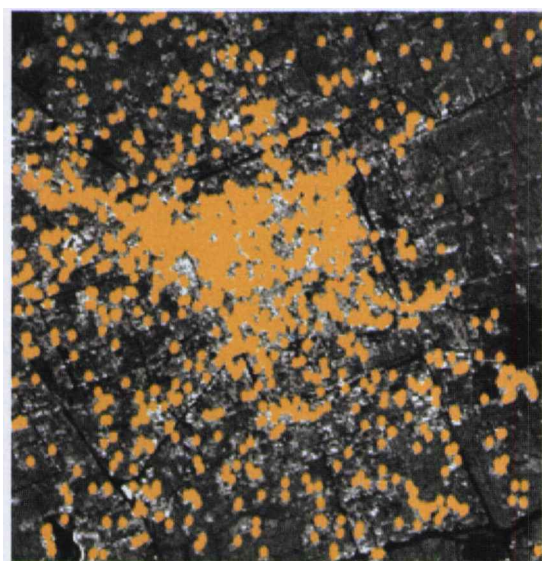

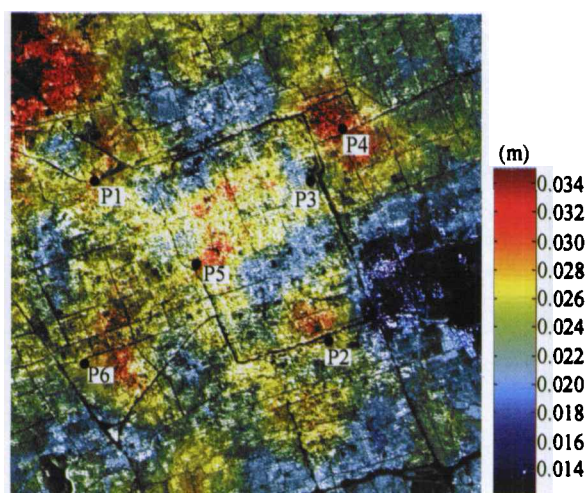Fig. 3. The distribution of the PSs over amplitude image.

Fig. 4. The deformation map over the test area using Kriging interpolation.

Table 2. Comparison of the result of PSInSAR with the leveling measurements at six benchmarks

	P_1	P_2	P_3	P_4	P_5	P_6
PSInSAR (1992—2000)	0.028 m	0.026 m	0.023 m	0.031 m	0.028 m	0.027 m
Leveling (1993—1995)	0.023 m	0.032 m	0.036 m	0.035 m	0.111 m	0.026 m

As a by-product of the PSs technique, the DEM error map and the estimated atmospheric phase screen of the master image are generated, as shown in Figs. 5 and 6, respectively.
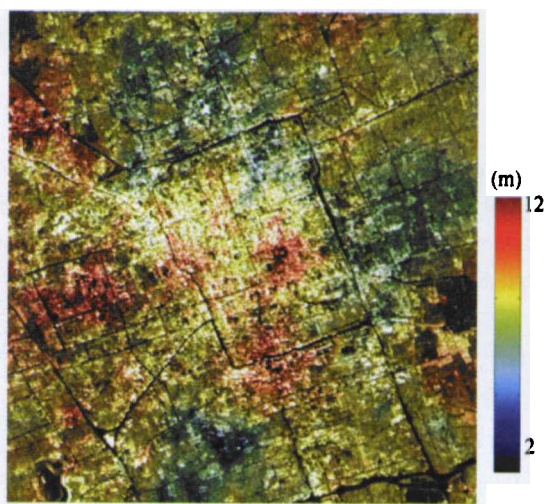

Fig. 5. The estimated DEM error map.

Fig. 6. The estimated atmospheric phase screen of the master image.

4 Conclusion and future work

To overcome the temporal decorrelation, the differential interferometric SAR based on permanent scatterers was carried out to retrieve the subsidence in

Suzhou city. The deformation rate map, DEM error map and atmospheric phase screen have been obtained. Because of the low-cost, large-cover and high-resolution characteristics of this technique, PS-DIn-SAR will be a great complement of the conventional geodetic tools, such as GPS and leveling to monitor the Earth surface movement over long time scales. Since ENVISAT was launched in 2002, the PS analysis on ERS interferometric data with ENVISAT ASAR images has become a major issue. This is ongoing and the experimental result will be shown in the near future.

References

1   Zebker H. A. and Goldstein R. Topographic mapping from SAR observation. J. Geophys. Res., 1996, 91(B5): 4993—4999.

2   Massonnet D. and amaud A. Deflation of Mount Etna monitored by space radar interferomety. Nature, 1995, 375: 567—570.

3   Zebker H. A. and Villasenor J. Decorrelation in interferometric radar echoes. IEEE Trans. Geosci. Remote Sensing, 1995, 22: 2517—2520.

4   Ferretti A., Prati C. and Rocca F. Non-linear subsidence rate estimation using permanent scatterers in differential SAR interferometry. IEEE Transactions on Geoscience and Remote Sensing, 2000, 38(5): 2202—2212.

5   Ferretti A., Prati C. and Rocca F. Permanent scatterers in SAR interferometry. IEEE Transactions on Geoscience and Remote Sensing, 2001, 39(1): 8—19.

6   Wang C., Zhang H., Liu Z. et al. Satellite SAR interferometric observations of displacement associated with urban subsidence in Suzhou Eastern China. Progress in Natural Science, 2002, 12(10): 798—801.

7   Wang C., Zhang H. and Liu Z. Spaceborne Interferometric Synthetic Aperture Radar (in Chinese). Beijing: Science Press, 2002.

8   Tarayre H. and Massonnet D. Effects of a refractive atmosphere on interferometric processing. In: IGARSS' 94, Pasadena, CA, 1994, 717—719.

9   Hanssen R. Radar Interferometry. Amsterdam, The Netherlands: Kluwer, 2001.

10   Marple S. L. Digital Spectral Analysis with Applications. Englewood Cliffs, NJ: Pretice-Hall, 1987.

11   Wang Z. R. Sustainable development suffering overexploitation of groundwater land subsidence and its conflicting in Suzhou-Wuxi-Changzhou area, Jiangsu Province. The Chinese Journal of Geological Hazard and Control (in Chinese), 1998, 2: 20—28.

12   Wang C., Zhang H., Liu Z. et al. Satellite SAR interferometric observations of displacement associated with urban subsidence in Suzhou Eastern China. Progress in Natural Science, 2002, 12(6): 621—624.